JBC Papers in Press. Published on October 12, 2006 as Manuscript M607079200
The latest version is at http://www.jbc.org/cgi/doi/10.1074/jbc.M607079200

Structural and Membrane Binding Analysis of the PX Domain of Phosphoinositide 3-Kinase-C2α*

Robert V. Stahelin[1], Dimitrios Karathanassis[2,5], Karol S. Bruzik[3], Michael D. Waterfield[4], Jerónimo Bravo[2,6], Roger L. Williams[2] and Wonhwa Cho[1]**

From the [1]Departments of Chemistry and [3]Medicinal Chemistry and Pharmacognosy, University of Illinois at Chicago, Chicago, IL 60607, USA, [2]MRC Laboratory of Molecular Biology, Cambridge CB2 2QH, UK, [4]Ludwig Institute of Cancer Research, University College, London W1p 8BT, UK,

Running Title: PI3K-C2α PX Domain Structure

[**]Address correspondence to: Wonhwa Cho, Department of Chemistry (M/C 111), University of Illinois at Chicago, 845 West Taylor Street, Chicago, Illinois 60607-7061; TEL: 312-996-4883; FAX: 312-996-2183; E-mail: wcho@uic.edu.

Current addresses: [5]Research Center For Biomaterials S.A. 15, 16562, Glyfada-Athens, Greece, [6]Centro Nacional de Investigaciones Oncológicas (CNIO), Melchor Fernández Almagro 3, E-28029 Madrid, Spain

Phox homology (PX) domains, which have been identified in a variety of proteins involved in cell signaling and membrane trafficking, have been shown to interact with phosphoinositides (PIs) with different affinities and specificities. To elucidate the structural origin of diverse PI specificities of PX domains, we determined the crystal structure of the PX domain from phosphoinositide 3-kinase C2α (PI3K-C2α), which binds phosphatidylinositol-4,5-bisphosphate (PtdIns(4,5)P_2). To delineate the mechanism by which this PX domain interacts with membranes, we measured the membrane binding of the wild type domain and mutants by surface plasmon resonance and monolayer techniques. This PX domain contains a signature PI-binding site that is optimized for PtdIns(4,5)P_2 binding. The membrane binding of the PX domain is initiated by nonspecific electrostatic interactions followed by the membrane penetration of hydrophobic residues. Membrane penetration is specifically enhanced by PtdIns(4,5)P_2. Furthermore, the PX domain displayed significantly higher PtdIns(4,5)P_2 membrane affinity and specificity when compared to the PI3K-C2α C2 domain, demonstrating that high affinity PtdIns(4,5)P_2 binding was facilitated by the PX domain in full-length PI3K-C2α. Together, these studies provide new structural insight into the diverse PI specificities of PX domains and elucidate the mechanism by which the PI3K-C2α PX domain interacts with PtdIns(4,5)P_2-containing membranes and thereby mediates the membrane recruitment of PI3K-C2α.

Numerous cellular processes including cell signaling and membrane trafficking involve complex arrays of protein-protein and lipid-protein interactions. Research in the past decade has revealed that a large number of cellular proteins reversibly translocate to specific subcellular locations to form lipid-protein interactions (1,2). These proteins, collectively known as peripheral proteins, typically contain one or more modular domains specialized in lipid binding (3,4). Common targets of many of these lipid binding domains are phosphoinositides (PIs)[1], which play a crucial role in cell signaling and membrane trafficking by serving as site-specific membrane signals to modulate the intracellular localization and/or biological activity of effector proteins (5-8) . PIs are metabolized by kinases and phosphatases, which catalyze the phosphorylation and dephosphorylation of PI at the 3', 4', or 5' position (9-12). PI 3-kinases (PI3Ks) are enzymes that catalyze the phosphorylation of phosphatidylinositol (PtdIns), phosphatidylinositol-4-phosphate (PtdIns4P), or phosphatidylinositol-4,5-bisphosphate

(PtdIns(4,5)P_2) at the 3' position of the inositol ring (13-15). PI3Ks are divided into 3 classes (class I, II, and III) based upon their structures and *in vitro* activities (16,17). Class II PI3K includes PI3K-C2α, PI3K-C2β, and PI3K-C2γ. These enzymes phosphorylate PtdIns and PtdIns4P at the 3' position *in vitro* (18-21) and act downstream of receptors for growth factors (22), chemokines (23), and integrins (24). Specifically, PI3K-C2α is activated by clathrin and has been shown to regulate clathrin-mediated membrane trafficking (25,26) as well as being essential for ATP-dependent priming of neurosecretory granule exocytosis (27). Class II PI3Ks harbor two membrane-targeting modules near their carboxy terminus, a Phox homology (PX) domain and a C2 domain. The PX domain of PI3K-C2α was reported to bind PtdIns(4,5)P_2 (28), while the C2 domain was reported to contain a nuclear localization signal (29) and bind PtdIns(4,5)P_2 and phosphatidylinositol-3,4-bisphosphate (PtdIns(3,4)P_2) (30). The roles and mutual interactions of these two domains in the membrane targeting and activation of PI3K-C2α still remain unknown.

The PX domain is a structural module composed of 100-140 amino acids that was first identified in the $p40^{phox}$ and the $p47^{phox}$ subunits of NADPH oxidase (31) and has since been found in a variety of other proteins involved in membrane trafficking (e.g., Mvp1p, Vps5p, Bem1p and Grd19p, and sorting nexins) and cell signaling (e.g., phospholipase D (PLD), PI3K, cytokine-independent survival kinase (CISK), and FISH) (32-34). Sequence comparisons of PX domains have shown that they contain several conserved regions, including a proline-rich stretch (PXXP) and a number of basic residues (32-34). Recently, PX domains have been shown to interact with different PIs and target the host proteins to different subcellular locations. Many PX domains, including those of Vam7p (35), sorting nexin 3 (36), and $p40^{phox}$ (37,38) specifically interact with phosphatidylinositol-3-phosphate (PtdIns3P) *in vitro* and also target the host proteins to early endosomes in the cell. In addition, most of yeast PX domains were reported to bind PtdIns3P, albeit with varying affinities (39). Unlike these PX domains, the PX domain of PI3K-C2α interacts with PtdIns(4,5)P_2 (28), while the $p47^{phox}$ PX domain preferentially interacts with PtdIns(3,4)P_2 (37). Also, the PX domains of the yeast protein Bem1p (40) and PLD1 (41) have specificity for PtdIns4P and phosphatidylinositol-3,4,5-trisphosphate (PtdIns(3,4,5)P_3), respectively. Recently, the PX domain of Nox organizing protein 1 was reported to bind PtdIns4P, phosphatidylinositol-5-phosphate (PtdIns5P), and phosphatidylinositol-3,5-bisphosphate (PtdIns(3,5)P_2) (42).

Recent structural and modeling studies of a variety of PX domains have provided insight into the stereospecific headgroup recognition and membrane binding mechanisms of PX domains. For example, the crystal structure of the $p40^{phox}$-PtdIns3P complex revealed that basic residues, Lys^{92} and Arg^{58}, specifically form hydrogen bonds with the 1- and 3-phosphate of PtdIns3P, respectively, thereby achieving the stereospecific recognition of PtdIns3P (43). The crystal structure of CISK-PX showed that this domain also has all the basic residues necessary for binding the 3-phosphate of PtdIns3P (44). The crystal structure of the PX domain of $p47^{phox}$ (45) revealed that this PX domain has two phospholipid binding sites for PtdIns(3,4)P_2 and phosphatidic acid (or phosphatidylserine), respectively. Similarly, a mutational and homology modeling study of the PLD1 PX domain suggested that it also has two binding sites; one specifically binding PtdIns(3,4,5)P_3 and the other interacting nonspecifically with anionic phospholipids (41). The crystal structures of free and PtdIns3P-bound PX domain of yeast Grd19p protein showed the lipid-induced local conformational changes involving putative membrane-penetrating hydrophobic residues (46).

To gain a better understanding of differential PI specificities and membrane-binding mechanisms of PX domains, we determined the X-ray crystal structure of the PI3K-C2α PX domain that was reported to specifically bind PtdIns(4,5)P_2 (28). We also measured the interaction of the PX domain and mutations with model membranes containing various PIs by surface plasmon resonance (SPR) and monolayer penetration analyses. In addition, we measured the PI-dependent membrane binding of the C2 domain and the full-length PI3K-C2α. Results from these studies provide new insight into how the PI3K-C2α PX domain specifically recognizes PtdIns(4,5)P_2 and how the PX and C2

domains mediate the PtdIns(4,5)P_2-dependent membrane targeting and activation of PI3K-C2α.

EXPERIMENTAL PROCEDURES

Materials — 1-Palmitoyl-2-oleoyl-*sn*-glycero-3-phosphate (POPA), 1-palmitoyl-2-oleoyl-*sn*-glycero-3-phosphocholine (POPC), 1-palmitoyl-2-oleoyl-*sn*-glycero-3-phosphoserine (POPS), and 1-palmitoyl-2-oleoyl-*sn*-glycero-phosphoethanolamine (POPE) were from Avanti Polar Lipids (Alabaster, AL). PtdIns3P, PtdIns4P, PtdIns5P, PtdIns(3,4)P_2, PtdIns(3,5)P_2, PtdIns(4,5)P_2, and PtdIns(3,4,5)P_3 were synthesized as described previously (47). Phospholipid concentrations were determined by a modified Bartlett analysis (48). The Liposofast microextruder and 100 nm polycarbonate filters were from Avestin (Ottawa, Ontario). Fatty acid-free bovine serum albumin was from Bayer, Inc. (Kankakee, IL). Restriction endonucleases and other enzymes for molecular biology were from New England Biolabs (Beverly, MA). [3-(3-cholamidopropyl) dimethylammonio]-1-propane-sulfonate (CHAPS) and octyl glucoside were from Sigma and Fisher Scientific, respectively. Pioneer L1 sensor chip was from Biacore AB (Piscataway, NJ).

Structure Determination — For the structure determination, DNA encoding the human PI3K-C2α PX domain (residues 1405 to 1541) was amplified by polymerase chain reaction (PCR) from IMAGE clone 825260 and subsequently cloned with a C-terminal GSH_6 affinity tag in pJL vector. The cloned PX domain was sequenced and showed two differences with respect to the only published human sequence of PI3K-C2α (accession id NP_002636). Residue 1450 is Arg in our sequence instead of Trp, and residue 1464 is an Asp instead of Val. Residue 1464 is critical for the lipid specificity of PX domains (see below). All of the PI3K-C2α sequences that have been reported have an Asp at the position equivalent to human PI3K-C2α residue 1464, and all of the PI3K-C2β and PI3K-C2γ sequences have a Glu at this position. Residue 1450 corresponds to a more variable region among PX domains in general, but it is an Arg in all other mammalian PI3K-C2 sequences. Consequently, it is likely that these differences with respect to the database reflect errors in the database entry.

The protein was expressed in *Escherichia coli* strain C41(DE3) and purified by Ni^{2+}-affinity, heparin and gel-filtration chromatography as described in Supplementary Methods. The protein in gel-filtration buffer (20 mM Tris-HCl (pH 7.4 at 25°C), 100 mM NaCl and 5 mM dithiothreitol) was concentrated to 5 mg/ml. Crystals were obtained by hair seeding drops (3 μl protein plus 3 μl reservoir solution) that were incubated at 17°C over a reservoir consisting of 1.7 M Li_2SO_4 and 0.05 M MES (pH 5.6). For the hair seeding, a hair from a poodle was passed through a drop with crystals then passed through a series of six freshly set up drops with no crystals so that the number of nuclei would thereby be serially diluted. When passing through each of the six drops, a pattern of an "X" was traced through the drop with the hair. In most cases, the first drop of the series had a shower of small crystals along the path of the hair and in the later drops in the series, only a few crystals were formed, but these were much larger. Crystals were visible after 24 h and grew to full size within one week.

For diffraction data collection, crystals were cryoprotected in reservoir solution supplemented with 15% glycerol and were flash frozen in a nitrogen stream at 100K. A heavy metal derivative crystal was prepared by soaking a crystal in cryoprotectant supplemented with 1 mM ethylmercury thiosalicylate (EMTS) for 15 min. An initial, lower resolution, 2.9 Å native data set was also collected and used for initial single isomorphous replacement phasing. Table I summarizes the data collection statistics. Images were processed with the program MOSFLM (49) and refined with SCALA (50) Three mercury sites were located with RANTAN and refined with AutoSHARP. After density modification with SOLOMON (51) and DM (52), an initial model was manually built in a 2.9 Å resolution electron density map using COOT (53)and O (54). A subsequent 2.6 Å data set was obtained for a native crystal, and this data set was used for refinement with REFMAC(55). There is one PX domain in the asymmetric unit. The Ramachandran analysis with the program PROCHECK (56) shows 88.8% of residues in the most probable regions and none in disallowed regions. The refinement statistics are given in Table I. A representative section of the experimental and refined electron densities are

illustrated in Supplemental Fig. 1. The coordinates have been deposited in the Protein Data Bank (accession number 2iwl).

Mutagenesis and Protein Expression — Mutagenesis of the PI3K-C2α PX domain was performed using the overlap extension PCR method (57). Constructs were subcloned into the pET21a vector containing a C-terminal hexahistidine tag and transformed into DH5α cells for plasmid isolation. After checking each construct for correct sequence, the plasmid was transformed into BL21(DE3) cells for protein expression. The PX domains used for monolayer and SPR measurements were expressed and purified as described previously (58) with minor variation: i.e., the domains purified by nickelnitrilotriacetic acid column were further purified by gel filtration chromatography. Briefly, a 1 ml sample of each PX domain was loaded onto a Superdex 200 column (Amersham-Pharmacia) equilibrated and eluted with 20 mM Tris-HCl buffer, pH 7.4, containing 0.16 M KCl. Fractions corresponding to the PI3K-C2α PX peak were pooled and concentrated to 1 ml. The C2 domain (residue 1562 to 1679) was cloned into pET21a using *Nde*I and *Xho*I sites. For C2 domain expression, BL21(DE3) cells were grown at 37°C in LB media containing 100 g /ml ampicillin. Protein expression was induced when the absorbance at 600 nm reached 0.8 and continued for 4 h at 25°C. Cells were pelleted by centrifugation and the C2 domain was purified as previously described (59). The full-length PI3K-C2α was expressed in Sf9 cells, purified, and assayed as previously described (21). Protein concentration was determined by the bicinchoninic acid method (Pierce).

Monolayer Measurements — The penetration of PI3K-C2α and isolated domains into the phospholipid monolayers of different lipid compositions was measured in terms of the change in surface pressure (π) using a 10-ml circular Teflon trough and a Wilhelmy plate connected to a Cahn microbalance as previously described (60).

SPR Measurements — All SPR measurements were performed at 23 °C in 10 mM HEPES, pH 7.4, containing 0.16 M KCl. A detailed protocol for coating the L1 sensor chip with lipid vesicles was reported previously (61,62) Briefly, after washing the sensor chip surface with the buffer, 90 μl of vesicles composed of POPC/POPE/PI (78:20:2) (see Fig. 3) were injected at 5 μl/min to give a response of 5500 resonance units (RU). Similarly, a control surface was coated with POPC/POPE (80:20) vesicles, to give the same resonance unit response as the active binding surface. Under our experimental conditions, no binding was detected to this control surface beyond the refractive index change for all proteins. Each lipid layer was washed with 10 μl of 50 mM NaOH three times at 100 μl/min. Typically, no decrease in lipid signal was seen after the first injection. Equilibrium (steady-state) SPR measurements were performed with the flow rate of 5 μl/min to allow sufficient time for the *R* values of the association phase to reach saturating response values (R_{eq}) (62,63). After sensorgrams were obtained for 5 different concentrations of each protein within a 10-fold range of K_d (see Table II), each of the sensorgrams was corrected for refractive index change by subtracting the control surface response from it. R_{eq} values were then plotted versus protein concentrations (C), and the K_d value was determined by a nonlinear least-squares analysis of the binding isotherm using an equation, $R_{eq} = R_{max}/(1 + K_d/C)$. Each data set was repeated three times to calculate average and standard deviation values.

RESULTS

Description of the Overall Structure — Unlike p40^{phox}, Vam7p, and Grd19p PX domains, PI3K-C2α has been reported to bind PtdIns(4,5)P_2 (28). To elucidate the basis of stereospecific recognition of PtdIns(4,5)P_2 by the PI3K-C2α PX domain, we determined its crystal structure by X-ray diffraction analysis.

The PI3K-C2α PX domain crystallized in space group P423 with a=115.9 Å and one molecule *per* asymmetric unit. Residues 1405-1408, 1488-1497 and 1540-1541 are disordered. The fold of the PI3K-C2α PX domain consists of a three-stranded meander β-sheet subdomain followed by a helical subdomain with four α-helices and one 3_{10} helix (Fig. 1A). The β-sheet is twisted by the bulge at residues 1430 and 1431 in strand β1. This twist of the β-sheet toward the helical sub-domain enables the formation of a pocket bordered on one side by

the beginning of strand β2. A sulfate is bound in this pocket on the surface of the domain and interacts with Arg[1503] of helix α3.

The PI3K-C2α PX domain superimposes closely on other PX domains such as the PX domain from p40*phox* (Fig. 1B). However, a loop immediately following the PXXP motif at residues 1483-1486 is disordered in the PI3K-C2α PX domain (shown as dashed line in Fig. 1A,B). This disorder gives the lipid-binding pocket a much more open appearance compared to the analogous pocket of p40*phox*. The core of the β-sheet subdomain is nearly identical among PX domains. However, the β1–β2 turn in the PI3K-C2α PX domain has a *cis*-proline (Pro[1438]), accentuating the curvature of the concave face of the β-sheet relative to other PX domains.

The comparison of the lipid-binding sites from p40*phox* (43) and PI3K-C2α PX domains immediately reveals why it would be impossible for PtdIns3P to bind the PI3K-C2α PX domain. Both negative selection against the 3-phosphate and loss of positive selection for the 3-phosphate contribute to the lipid specificity of the PI3K-C2α PX domain. Figs. 2A and 2B illustrate that positive selection is lost because the essential, conserved determinant of the 3-phosphate interaction, which is Arg[58] in p40*phox*, has been replaced by Thr[1462] in PI3K-C2α. Arg[60] of the p40*phox* PX domain, which is one of the residues responsible for its 1-phosphate coordination, has been replaced in PI3K-C2α by Asp[1464], The orientation of Asp[1464] is such that it imposes a negative selection against 3-phosphate, as it would electrostatically repel a phosphate.

The PP_{II}/α2 loop is disordered in the PX domain structure, preventing us from suggesting a detailed model of PtdIns(4,5)P_2 binding to PI3K-C2α PX domain. However, the bound sulfate molecule in the PI3K-C2α PX domain seems to indicate a plausible position of 4-phosphate binding. The sulfate in PI3K-C2α is hydrogen bonded to Arg[1503], which superimposes well with the p40*phox* residue (Arg[105]) that interacts with the 4- and 5-OH of PtdIns3P. In the PI3K-C2α PX domain structure, there is no clear indication for a 5-phosphate specificity determinant. However, a few candidate residues could be suggested as illustrated in Fig. 2B. In the p40*phox* and Grd19 PX domains, the backbone of the variable loop between PP_{II} and α2 embraces the 4- and 5-OH of the bound phosphoinositide and the side chain of a basic residue analogous to Arg[1503] in helix α2 of PI3K-C2α interacts with these groups (Fig. 2B). Consequently, basic residues in the variable loop or at the beginning of helix α2 are likely possibilities as 5-phosphate ligands. Arg[1488], Arg[1493] and Lys[1497] are such candidates. Another possibility might be Lys[1440] from the β1/β2 loop. The fact that the variable PP_{II}/α2 loop is disordered indicates an accented flexibility, suggesting that lipid binding may confer localized conformational changes enabling Lys[1440], Arg[1488], Arg[1493], or Lys[1497] to point towards the lipid-binding pocket. Indeed, studies of the Grd19 PX domain in the absence and presence of PtdIns3P show that the PP_{II}/α2 loop closes in on the bound lipid (46). The variable PP_{II}/α2 loops of p40*phox* and Grd19 also provide the 1-phosphate ligand (Fig. 2B).

Intramolecular interactions between polyproline regions and SH3 domains have been previously reported for several proteins, including p47*phox* (45). It appears that for such intramolecular interactions to occur in PX domains a type I polyproline motif is required. The p40*phox*, Grd19, and PI3K-C2α PX domains all contain polyproline regions, which feature the PxxPxR(K) consensus, which corresponds to the type II SH3-ligand motif PxxPx+ (where + refers to a positively charged amino acid and x to any residue). In p40*phox*-PX the last residue of the motif, Lys[92], participates in lipid-recognition. The equivalent residue in PI3K-C2α-PX, Arg[1488], is disordered, but it is possible that Arg[1488] might become ordered on lipid binding, and it may be that this residue is the 1-phosphate ligand (Fig. 2B). In all three proteins, the prolines of the PXXP loop are buried. PI3K-C2α isoforms do not contain SH3 domains, and to date there has been no report of an interaction between PI3K-C2α and the SH3 domain from another protein. These observations suggest that perhaps type II SH3-ligand motifs in PX domains are not sufficient on their own to mediate interactions with SH3 domains.

Membrane Binding Properties — To determine the functional roles of the putative phospholipid binding residues of PI3K-C2α PX, we measured the vesicle binding of wild type and a series of site-specific mutants by SPR and monolayer penetration analyses. We first measured

the PI specificity of PI3K-C2α PX domain by SPR analysis. In these experiments, an active surface was coated with POPC/POPE/PI (75:20:5), while a control surface was coated with POPC/POPE (80:20). Fig. 3 shows the binding response changes for 500 nM of PI3K-C2α PX injected over various PI-containing membranes. Clearly, PI3K-C2α PX has specificity for PtdIns(4,5)P_2-containing vesicles, as it exhibited no significant binding to all other membranes. Fig. 4A shows representative sensorgrams for equilibrium binding analysis of PI3K-C2α PX-POPC/POPE/PtdIns(4,5)P_2 (78:20:2) vesicle binding, and K_d values determined from the curve fitting (Fig. 4B) are summarized in Table II. The affinity of the PI3K-C2α PX domain for PX-POPC/POPE/PtdIns(4,5)P_2 (78:20:2) vesicles (K_d = 25 nM) is higher than that of an archetypal PtdIns(4,5)P_2 binding domain, the PH domain of phospholipase Cδ1 (1-8 μM) (64,65) and comparable to the ENTH domain of epsin 1(66).

We then measured the binding of PI3K-C2α PX mutants to POPC/POPE/PtdIns(4,5)P_2 (78:20:2) vesicles. In agreement with the structural analysis, the mutation of the conserved Arg^{1503} (i.e., R1503A) abolished binding to PtdIns(4,5)P_2-containing membranes, corroborating the notion that this conserved Arg residue is essential for recognition of PtdIns(4,5)P_2 and may interact with the 4-phosphate. Mutations of two other basic residues, Arg^{1488} and Arg^{1493}, that are candidates for 5-phosphate recognition in the PtdIns(4,5)P_2-binding pocket of PI3K-C2α PX (R1488A and R1493A) reduced the vesicle affinity of the PX domain by 7- and 23-fold, respectively, whereas mutations of other neighboring residues (K1440A and K1497A) had little effect. This indicates that Arg^{1488} and Arg^{1493}, in addition to Arg^{1503}, may be involved in specific PtdIns(4,5)P_2 recognition. Gross misfolding was precluded for all mutations as they were expressed at the same level as wild type and bound POPC/POPS (5:5) vesicles with the same affinity as wild type (data not shown).

Recently, it has been shown that hydrophobic residues surrounding the PI binding pockets of FYVE (67,68), PX (46,58), and ENTH (66,69) domains can penetrate the membrane following PI binding. We thus measured the effects of mutations of hydrophobic residues (Val^{1490} and Leu^{1491}) surrounding the PI-binding pocket of the PI3K-C2α PX domain to see if they are involved in membrane penetration. V1490A and L1491A exhibited a 7- and 5-fold lower membrane affinity than the wild type, respectively. Interestingly, mutation of Leu^{1479}, which is located on the same molecular surface with Val^{1490} and Leu^{1491} but distant from the PI binding pocket, had little effect on binding to PtdIns(4,5)P_2-containing vesicles. This indicates that only hydrophobic residues adjacent to the PI-binding pocket specifically penetrate the membrane (see below).

Membrane penetration properties of PI3K-C2α PX domain and mutants were further characterized by lipid monolayer penetration measurements. Recent studies have shown that PIs can specifically induce the membrane penetration of FYVE (68), PX (58), and ENTH (66,69) domains. To determine whether or not PtdIns(4,5)P_2 can also elicit the membrane penetration of the PI3K-C2α PX domain, we first measured the penetration of the PX domain to monolayers with different lipid compositions (see Fig. 5). The PI3K-C2α PX domain cannot penetrate the POPC/POPE (80:20) monolayer with the surface pressure above 26 dyne/cm; however, when 2 mol% PtdIns(4,5)P_2 was included in the monolayer (i.e., POPC/POPE/PtdIns(4,5)P_2 (78:20:2), the domain penetrated the monolayer with the surface pressure of up to 33 dyne/cm. Since the surface pressure of biological membranes has been estimated to be 30 to 35 dyne/cm (70-72), these data suggest that PtdIns(4,5)P_2 can induce the penetration of the PI3K-C2α PX domain into cell membranes under physiological conditions. The specific nature of this penetration was confirmed by two additional measurements. First, neither 2 mol% PtdIns(3,4)$_2$ nor 2 mol% PtdIns(3,4,5)P_3 nor 20 mol% PS in the monolayer significantly influence the penetration behaviors of PI3K-C2α PX. Second, mutations of residues involved in specific PtdIns(4,5)P_2 recognition (i.e., R1503A and R1488A) greatly reduced the penetration of the PI3K-C2α PX domain to the POPC/POPE/PtdIns(4,5)P_2 (78:20:2) monolayer while mutations which had no effect on K_d, K1440A and L1479A, did not cause reduction in monolayer penetration (Fig. 6A). Lastly, V1490A and L1491A had low monolayer penetration into the POPC/POPE/PtdIns(4,5)P_2 (78:20:2) monolayer (Fig. 6B), confirming the notion that these hydrophobic residues are directly involved in the membrane penetration of the PI3K-

C2α PX domain. In contrast, the mutation of Leu[1479] located at the other end of the membrane-binding surface had little effect on the monolayer penetration (Fig. 6B), showing that this part of PI3K-C2α PX does not significantly participate in membrane penetration.

PtdIns(4,5)P_2 Binding of C2 Domain versus PX Domain — The recent study of the C2 domain of PI3K-C2α indicated that it had affinity for PIs, particularly PtdIns(4,5)P_2 and PtdIns(3,4)P_2 (30). This finding raises a question as to whether the PX domain or the C2 domain plays a major role in PI-mediated membrane binding of PI3K-C2α. In order to compare the PI specificities and affinities of the PX and C2 domains, we measured the binding of the C2 domain to PI-containing vesicles by SPR analysis and also monitored their binding to PI-containing lipid monolayers.

We first measured the PI specificity of PI3K-C2α C2 domain by SPR analysis using the active surface coated with POPC/POPE/PI (75:20:5) vesicles. A control surface was coated with POPC/POPE (80:20) vesicles. Fig. 7 shows the binding response changes for 500 nM of the PI3K-C2α C2 domain injected over various PI-containing membranes. In agreement with the previous report (30), the PI3K-C2α C2 domain binds PtdIns(3,4)P_2 and PtdIns(4,5)P_2; however, unlike the PX domain, the C2 domain can significantly bind other PIs and consequently shows low PI selectivity. In fact, quantitative analysis of the binding data (see Table III) showed that the C2 domain could not effectively distinguish among various PIs. Perhaps more importantly, the affinity of the C2 domain for POPC/POPE/PtdIns(4,5)P_2 (78:20:2) (K_d ~ 490 nM) was about 20-fold lower than that of the PX domain (K_d ~ 25 nM) under the same conditions. We also measured the binding of the PX and C2 domains as a function of PtdIns(4,5)P_2 concentration (i.e., using POPC/ POPE/PtdIns(4,5)P_2 (80-*x*:20:*x*) vesicles). As shown in Fig. 8, the PX domain had higher affinity than the C2 domain throughout the PtdIns(4,5)P_2 concentration range used and the difference was the most dramatic at the physiologically relevant PtdIns(4,5)P_2 concentration (i.e., <5 mol%). Also, the PtdIns(4,5)P_2 concentration for half-maximal binding of the PX domain (~2 mol%) was significantly lower than that of the C2 domain (~7 mol%), and the latter is consistent with the reported value (30). Collectively, these results indicate that the PX domain would play a dominant role in PtdIns(4,5)P_2-mediated membrane binding of PI3K-C2α.

We then measured the monolayer penetration of the C2 domain to see if the domain shows significant membrane penetration and if PIs could induce the penetration of the C2 domain. Fig 9A illustrates that the C2 domain has much lower monolayer penetrating power than the PX domain in the presence of PtdIns(4,5)P_2 and the π_c value for the C2 domain was significantly lower than 30 dyne/cm. Also, unlike the case with PX domain, PtdIns(4,5)P_2 (or PtdIns(3,4)P_2) enhanced the monolayer penetration of the C2 domain only slightly. This again indicates that the PX domain should be a main player in all aspects of membrane interactions of PI3K-C2α, including membrane penetration.

PtdIns(4,5)P_2-Mediated Membrane Binding of the Full-Length PI3K-C2α — To verify the notion that the PX domain controls the membrane binding of PI3K-C2α, we prepared wild type and R1503A mutant (PtdIns(4,5)P_2 binding-defective; see Table II) of the full-length PI3K-C2α and compared their membrane binding properties with the isolated PX and C2 domains. R1503A was expressed as effectively as wild type in the Sf9 cells and had the basal activity comparable to that of wild type, precluding the gross misfolding of the mutant (data not shown). SPR analysis (see Table III) shows that the full-length PI3K-C2α and the isolated PX domain have essentially the same affinity for PtdIns(4,5)P_2-containing membranes (~20 nM), underscoring the predominant role of the PX domain in the membrane binding of PI3K-C2α. Interestingly, the R1503A mutant of the full-length protein had 25-fold lower affinity than the wild type, which was comparable to that of the isolated C2 domain. This suggests that the C2 domain supplements the function of PX domain in PtdIns(4,5)P_2-mediated membrane binding and that the two domains work additively rather than synergistically. Lastly, we compared the monolayer penetration of the full-length PI3K-C2α and the isolated PX domain (see Fig. 9B). PI3K-C2α penetrated the monolayer in a PtdIns(4,5)P_2-dependent manner similarly to the isolated PX

domain, while the R1503A mutation abrogated the PtdIns(4,5)P_2 dependent penetration, demonstrating that the PX domain is essential for the penetration of the full-length enzyme.

DISCUSSION

The present study addresses two important questions: how does the PX domain of PI3K-C2α specifically recognize PtdIns(4,5)P_2 and how does the PX domain mediate the membrane binding and activation of PI3K-C2α? PX domains are similar to PH domains in that they have highly variable PI specificities and affinities. High-resolution structures of several PX domains that bind the 3'-phosphate have been determined as either free proteins or complexes with PI (43-46). However, the structural information for the PX domains that specifically bind non-3'-phosphate-PI has not been available.

The crystal structure of the PI3K-C2α PX domain clearly accounts for its inability to bind PtdIns3P that most PX domains prefer. A canonical 3'-phosphate ligand (i.e., Arg^{58} for $p40^{phox}$ PX) is substituted for by Thr and an acidic residue, Asp^{1464}, replaces a 1'-phosphate ligand (i.e., Arg^{60} in $p40^{phox}$ PX). This negative selection would not allow PtdIns3P to favorably interact with the PI binding pocket of the PI3K-C2α PX domain. Due to the disorder in the PP_{II}/α2 loop of the PI3K-C2α PX domain, there is no direct structural information on how the domain achieves stereospecific recognition of the 4'- and 5'-phosphates of PtdIns(4,5)P_2. However, the location of a bound sulfate ion, sequence alignment, and our mutational analysis suggest that three basic residues, Arg^{1488}, Arg^{1493}, and Arg^{1503}, are involved in PtdIns(4,5)P_2 binding. Presumably, Arg^{1503} interacts with the 4'-phosphate whereas Arg^{1493} contacts the 5'-phosphate. Arg^{1488} may be involved in binding to either the 5'-phosphate or the 1'-phosphate.

Our previous studies on the FYVE (68), PX (58), and ENTH (66) domains have indicated that PI binding specifically induces the membrane penetration of surface hydrophobic residues surrounding the PI-binding pocket, presumably by causing local conformational changes of proteins and by neutralizing the positive electrostatic potential surrounding hydrophobic loop residues that interferes with the membrane penetration of domains. Based on these previous studies, we proposed a membrane binding mechanism for PI-binding domains in which initial membrane adsorption of the domain driven by nonspecific electrostatic interactions between the cationic protein surface and the anionic membrane surface is followed by specific PI-triggered membrane penetration of the domain. The present study indicates that PtdIns(4,5)P_2-mediated membrane binding of the PI3K-C2α PX domain follows essentially the same mechanism. Our monolayer data clearly indicate that PtdIns(4,5)P_2 binding by the PI3K-C2α PX domain is not a consequence of but a prerequisite for the penetration of the domain into the monolayer, the packing density of which is comparable with that of cellular membranes and large unilamellar vesicles (70-72). The penetration of hydrophobic residues (Val^{1490} and Leu^{1491}) located in the loop adjacent to the PtdIns(4,5)P_2-binding pocket of PI3K-C2α PX is a specific PtdIns(4,5)P_2-dependent process, since it was abrogated either by removal of PtdIns(4,5)P_2 in the monolayer or by mutation of the PtdIns(4,5)P_2-coordinating residues, Arg^{1488}, Arg^{1493}, or Arg^{1503}.

The present study provides no direct information as to whether or not PtdIns(4,5)P_2 binding causes conformational changes of the PI3K-C2α PX domain. Structural studies of other PX domains have indicated, however, that PI binding causes local conformational changes. For example, a recent NMR study on the PX domain of Vam7p revealed that residues in its putative membrane binding loops underwent large changes in chemical shift when dodecylphosphocholine micelles were added to the PX domain-PtdIns3P complex (35). Also, crystal structures of the Grd19p PX domain in the absence and presence of a bound PtdIns3P showed conformational differences in the putative membrane attachment loop (46). This, in conjunction with the PI3K-C2α PX domain structure showing high flexibility of the PP_{II}/α2 loop, suggests that PtdIns(4,5)P_2 binding may also induce the conformational change and thereby facilitate the membrane penetration of hydrophobic side chains.

On the basis of qualitative vesicle pelleting assay, a recent study indicated that the C2 domain of PI3K-C2α has high affinity and specificity for PtdIns(4,5)P_2 and PtdIns(3,4)P_2 (30). Our quantitative SPR measurements confirm that the C2

domain of PI3K-C2α can indeed bind PtdIns(4,5)P_2 and PtdIns(3,4)P_2; however, the C2 domain lacks PI specificity and has about 20-fold lower affinity for PtdIns(4,5)P_2-containing vesicles than the PX domain. The promiscuity and lower affinity of the C2 domain for PIs has been reported for other C2 domains from synaptotagmin I (73), JFC1 (74), and Rsp5p (75). Also, unlike the PX domain, the C2 domain of PI3K-C2α is not able to penetrate the lipid monolayer with the packing density comparable to that of cell membranes with or without PI. Furthermore, the isolated PX domain and the full-length PI3K-C2α have comparable affinity for PtdIns(4,5)P_2-containing monolayers and bilayers. Thus, it is evident that the PX domain plays a more dominant role than the C2 domain in the PtdIns(4,5)P_2-mediated membrane recruitment of PI3K-C2α. It should be noted, however, that promiscuous PI specificity of the C2 domain may allow this domain to play a more significant role in the membrane recruitment of PI3K-C2α in response to PIs other than PtdIns(4,5)P_2. It is also possible that the membrane recruitment of PI3K-C2α is mediated by both the PX domain and the C2 domain, interacting with PtdIns(4,5)P_2 and another PI, respectively. Interestingly, the C2 domain of PI3K-C2α harbors a nuclear localization sequence and associates with nuclear speckles (29). Further studies are needed to understand how the nuclear localization signal and the lipid binding site of the C2 domain are related.

It is generally thought that specific subcellular localization of PI3K-C2α is critical for spatiotemporal regulation of the formation of 3'-phospho-PIs. While the present study clearly shows that the PX domain drives the binding of PI3K-C2α to PtdIns(4,5)P_2-containing membranes in vitro, the role of the PX domain (and the C2 domain) in the subcellular localization of PI3K-C2α remains less clear. In particular, two recent reports indicate that protein-protein interactions play a primary role in subcellular localization of PI3K-C2α. Domin et al. (76) reported that PI3K-C2α was enriched in clathrin-coated vesicles and trans-Golgi network of various mammalian cells but that neither the PX domain nor the C2 domain was necessary for this observed subcellular localization. Also, Gaidarov et al. (25) reported that clathrin bound the N-terminal region of PI3K-C2α and thereby activated the enzyme. This apparent discrepancy between the in vitro membrane binding properties and subcellular localization of PI3K-C2α is not totally surprising, however, as similar observations have been made for other peripheral proteins. For example, a study of all PH domains from the yeast genome showed that PI affinity, while contributing to membrane binding, does not specify subcellular localization (77). As a matter of fact, accumulating evidence shows that the subcellular localization of many peripheral proteins, including those proteins that were known to be recruited to the membrane primarily by protein-protein interactions, is orchestrated by a combination of protein-protein and lipid-protein interactions, and that the relative contribution of two types of interactions varies among proteins (1,78). It should be also noted that an interaction that appears to make a minor contribution in terms of the overall energetics of subcellular targeting of a protein may play a pivotal role in regulating its subcellular localization and activities (1,78).

For PI3K-C2α, protein-protein interactions involving its N-terminal region may play a major role in subcellular localization, but the membrane interactions by the PX domain (and the C2 domain) should also contribute significantly. PtdIns(4,5)P_2 is present in significant concentrations in the plasma membrane (ca. 1 mol%) and internal membranes and can be locally enriched (79). In particular, clathrin-coated pits in the plasma membrane are known to have a high local PtdIns(4,5)P_2 concentration (80-83). The affinity of the PI3K-C2α PX domain for PtdIns(4,5)P_2 is similar to that of other PtdIns(4,5)P_2-binding domains, including the ENTH domain of epsin1 (66), which were shown to recruit their respective host proteins to the PtdIns(4,5)P_2-rich region in the plasma membrane. Thus, it is reasonable to postulate that the PX domain of PI3K-C2α should make a contribution to the binding of PI3K-C2α to PtdIns(4,5)P_2-rich cell membranes, including clathrin-coated pits, clathrin-coated vesicles, and possibly the trans-Golgi network. Another salient feature of the PX domain to be considered in terms of enzyme activation is the PtdIns(4,5)P_2-mediated membrane penetration. It has been shown that triggering and sustaining the catalytic activity of many lipid-dependent enzymes, such as protein kinases C (84,85) and phospholipases (60), involves partial membrane penetration of their lipid binding domains.

Therefore, it is possible that the PtdIns(4,5)P_2-mediated membrane penetration of the PX domain is a part of the activation process for PI3K-C2α and/or is necessary for the processive enzymatic action at the membrane. Additionally, the promiscuous C2 domain could also play a role of prolonging membrane residence of PI3K-C2α while the local concentration of 3'-phospho-PIs increases as a result of PI3K-C2α action. Undoubtedly, further studies are necessary to fully understand the relative importance of protein-protein versus lipid-protein interactions in the subcellular localization and activation of PI3K-C2α.

In summary, the present investigation elucidates the structural basis of specific PtdIns(4,5)P_2 recognition by the PI3K-C2α PX domain and the mechanism by which the PX domain interacts with PtdIns(4,5)P_2-containing membranes. This, in conjunction with our previous work on other PX domains, shows that PX domains achieve unique modes of ligand and membrane binding through the variation of a limited number of non-conserved residues. This work may serve as a framework with which to systematically study the mechanism of specific membrane recruitment and regulation of PI3K-C2α as well as to comprehensively study the effects of structural and functional diversity of PX domains on lipid-protein and protein-protein interactions during cell signaling and membrane trafficking.

Acknowledgments — The expert assistance of Joanne McCarthy with ESRF beamline ID14-2 is gratefully acknowledged. We thank Olga Perisic for assistance with the structural work and for critically reviewing the manuscript.

REFERENCES

1. Cho, W. (2006) *Sci STKE* **2006**, pe7
2. Teruel, M. N., and Meyer, T. (2000) *Cell* **103**, 181-184
3. DiNitto, J. P., Cronin, T. C., and Lambright, D. G. (2003) *Sci STKE* **2003**, re16
4. Cho, W., and Stahelin, R. V. (2005) *Annu Rev Biophys Biomol Struct* **34**, 119-151
5. Cremona, O., and De Camilli, P. (2001) *J Cell Sci* **114**, 1041-1052
6. Czech, M. P. (2003) *Annu Rev Physiol* **65**, 791-815
7. Toker, A. (2002) *Cell Mol Life Sci* **59**, 761-779
8. Roth, M. G. (2004) *Physiol Rev* **84**, 699-730
9. Leslie, N. R., Biondi, R. M., and Alessi, D. R. (2001) *Chem Rev* **101**, 2365-2380
10. Comer, F. I., and Parent, C. A. (2002) *Cell* **109**, 541-544
11. Cantrell, D. A. (2001) *J Cell Sci* **114**, 1439-1445
12. Rameh, L. E., and Cantley, L. C. (1999) *J Biol Chem* **274**, 8347-8350
13. Czech, M. P. (2000) *Cell* **100**, 603-606
14. Cantley, L. C. (2002) *Science* **296**, 1655-1657
15. Lindmo, K., and Stenmark, H. (2006) *J Cell Sci* **119**, 605-614
16. Fruman, D. A., Meyers, R. E., and Cantley, L. C. (1998) *Annu Rev Biochem* **67**, 481-507
17. Domin, J., and Waterfield, M. D. (1997) *FEBS Lett* **410**, 91-95
18. MacDougall, L. K., Domin, J., and Waterfield, M. D. (1995) *Curr Biol* **5**, 1404-1415
19. Molz, L., Chen, Y. W., Hirano, M., and Williams, L. T. (1996) *J Biol Chem* **271**, 13892-13899.
20. Virbasius, J. V., Guilherme, A., and Czech, M. P. (1996) *J Biol Chem* **271**, 13304-13307
21. Domin, J., Pages, F., Volinia, S., Rittenhouse, S. E., Zvelebil, M. J., Stein, R. C., and Waterfield, M. D. (1997) *Biochem J* **326**, 139-147
22. Brown, R. A., Domin, J., Arcaro, A., Waterfield, M. D., and Shepherd, P. R. (1999) *J Biol Chem* **274**, 14529-14532
23. Turner, S. J., Domin, J., Waterfield, M. D., Ward, S. G., and Westwick, J. (1998) *J Biol Chem* **273**, 25987-25995
24. Zhang, J., Banfic, H., Straforini, F., Tosi, L., Volinia, S., and Rittenhouse, S. E. (1998) *J Biol Chem* **273**, 14081-14084
25. Gaidarov, I., Smith, M. E., Domin, J., and Keen, J. H. (2001) *Mol Cell* **7**, 443-449
26. Gaidarov, I., Zhao, Y., and Keen, J. H. (2005) *J Biol Chem* **280**, 40766-40772
27. Meunier, F. A., Osborne, S. L., Hammond, G. R., Cooke, F. T., Parker, P. J., Domin, J., and Schiavo, G. (2005) *Mol Biol Cell* **16**, 4841-4851
28. Song, X., Xu, W., Zhang, A., Huang, G., Liang, X., Virbasius, J. V., Czech, M. P., and Zhou, G. W. (2001) *Biochemistry* **40**, 8940-8944.
29. Didichenko, S. A., and Thelen, M. (2001) *J Biol Chem* **276**, 48135-48142
30. Liu, L., Song, X., He, D., Komma, C., Kita, A., Virbasius, J. V., Huang, G., Bellamy, H. D., Miki, K., Czech, M. P., and Zhou, G. W. (2006) *J Biol Chem* **281**, 4254-4260
31. Ponting, C. P. (1996) *Protein Sci* **5**, 2353-2357
32. Wishart, M. J., Taylor, G. S., and Dixon, J. E. (2001) *Cell* **105**, 817-820.
33. Xu, Y., Seet, L. F., Hanson, B., and Hong, W. (2001) *Biochem J* **360**, 513-530.
34. Ellson, C. D., Andrews, S., Stephens, L. R., and Hawkins, P. T. (2002) *J Cell Sci* **115**, 1099-1105.
35. Cheever, M. L., Sato, T. K., de Beer, T., Kutateladze, T. G., Emr, S. D., and Overduin, M. (2001) *Nat Cell Biol* **3**, 613-618.
36. Xu, Y., Hortsman, H., Seet, L., Wong, S. H., and Hong, W. (2001) *Nat Cell Biol* **3**, 658-666.
37. Kanai, F., Liu, H., Field, S. J., Akbary, H., Matsuo, T., Brown, G. E., Cantley, L. C., and Yaffe, M. B. (2001) *Nat Cell Biol* **3**, 675-678.
38. Ellson, C. D., Gobert-Gosse, S., Anderson, K. E., Davidson, K., Erdjument-Bromage, H., Tempst, P., Thuring, J. W., Cooper, M. A., Lim, Z. Y., Holmes, A. B., Gaffney, P. R., Coadwell, J., Chilvers, E. R., Hawkins, P. T., and Stephens, L. R. (2001) *Nat Cell Biol* **3**, 679-682.

39. Yu, J. W., and Lemmon, M. A. (2001) *J Biol Chem* **276**, 44179-44184
40. Ago, T., Takeya, R., Hiroaki, H., Kuribayashi, F., Ito, T., Kohda, D., and Sumimoto, H. (2001) *Biochem Biophys Res Commun* **287**, 733-738.
41. Stahelin, R. V., Ananthanarayanan, B., Blatner, N. R., Singh, S., Bruzik, K. S., Murray, D., and Cho, W. (2004) *J Biol Chem* **279**, 54918-54926
42. Cheng, G., and Lambeth, J. D. (2004) *J Biol Chem* **279**, 4737-4742
43. Bravo, J., Karathanassis, D., Pacold, C. M., Pacold, M. E., Ellson, C. D., Anderson, K. E., Butler, P. J., Lavenir, I., Perisic, O., Hawkins, P. T., Stephens, L., and Williams, R. L. (2001) *Mol Cell* **8**, 829-839.
44. Xing, Y., Liu, D., Zhang, R., Joachimiak, A., Songyang, Z., and Xu, W. (2004) *J Biol Chem*
45. Karathanassis, D., Stahelin, R. V., Bravo, J., Perisic, O., Pacold, C. M., Cho, W., and Williams, R. L. (2002) *Embo J* **21**, 5057-5068.
46. Zhou, C. Z., de La Sierra-Gallay, I. L., Quevillon-Cheruel, S., Collinet, B., Minard, P., Blondeau, K., Henckes, G., Aufrere, R., Leulliot, N., Graille, M., Sorel, I., Savarin, P., de la Torre, F., Poupon, A., Janin, J., and van Tilbeurgh, H. (2003) *J Biol Chem* **278**, 50371-50376
47. Bruzik, K. S., and Kubiak, R. J. (1995) *Tetrahedron Lett* **36**, 2415-2418
48. Kates, M. (1986) *Techniques of Lipidology*, 2nd Ed., Elsevier, Amsterdam
49. Leslie, A. G. W. (1992) in *Joint CCP4 and ESF-EACMB Newsletter on Protein Crystallography*, Daresbury Laboratory, Warrington, UK
50. Collaborative Computational Project, N. (1994) *Acta Cryst.* **D50**, 760-763
51. Abrahams, J. P., and Leslie, A. G. W. (1996) *Acta Cryst.* **D52**, 30-42
52. Cowtan, K., and Main, P. (1998) *Acta Cryst.* **D54**, 487-493
53. Emsley, P., and Cowtan, K. (2004) *Acta Cryst.* **D60**, 2126-2132
54. Jones, T. A., Zou, J.-Y., Cowan, S. W., and Kjeldgaard, M. (1991) *Acta Cryst.* **A47**, 110-119.
55. Murshudov, G. N., Vagin, A. A., and Dodson, E. J. (1997) *Acta Cryst.* **D53**, 240-255
56. Laskowski, R. A., MacArthur, M. W., Moss, D. S., and Thornton, J. M. (1993) *J Appl Cryst* **26**, 283-291.
57. Ho, S. N., Hunt, H. D., Horton, R. M., Pullen, J. K., and Pease, L. R. (1989) *Gene* **77**, 51-59
58. Stahelin, R. V., Burian, A., Bruzik, K. S., Murray, D., and Cho, W. (2003) *J Biol Chem* **278**, 14469-14479
59. Stahelin, R. V., and Cho, W. (2001) *Biochem J* **359**, 679-685.
60. Bittova, L., Sumandea, M., and Cho, W. (1999) *J Biol Chem* **274**, 9665-9672.
61. Bittova, L., Stahelin, R. V., and Cho, W. (2001) *J Biol Chem* **276**, 4218-4226.
62. Stahelin, R. V., and Cho, W. (2001) *Biochemistry* **40**, 4672-4678.
63. Ananthanarayanan, B., Stahelin, R. V., Digman, M. A., and Cho, W. (2003) *J Biol Chem* **278**, 46886-46894
64. Lemmon, M. A., Ferguson, K. M., O'Brien, R., Sigler, P. B., and Schlessinger, J. (1995) *Proc Natl Acad Sci U S A* **92**, 10472-10476
65. Kavran, J. M., Klein, D. E., Lee, A., Falasca, M., Isakoff, S. J., Skolnik, E. Y., and Lemmon, M. A. (1998) *J Biol Chem* **273**, 30497-30508
66. Stahelin, R. V., Long, F., Peter, B. J., Murray, D., De Camilli, P., McMahon, H. T., and Cho, W. (2003) *J Biol Chem* **278**, 28993-28999
67. Kutateladze, T., and Overduin, M. (2001) *Science* **291**, 1793-1796.
68. Stahelin, R. V., Long, F., Diraviyam, K., Bruzik, K. S., Murray, D., and Cho, W. (2002) *J Biol Chem* **277**, 26379-26388.
69. Ford, M. G., Mills, I. G., Peter, B. J., Vallis, Y., Praefcke, G. J., Evans, P. R., and McMahon, H. T. (2002) *Nature* **419**, 361-366
70. Demel, R. A., Geurts van Kessel, W. S., Zwaal, R. F., Roelofsen, B., and van Deenen, L. L. (1975) *Biochim Biophys Acta* **406**, 97-107.
71. Blume, A. (1979) *Biochim Biophys Acta* **557**, 32-44.
72. Marsh, D. (1996) *Biochim Biophys Acta* **1286**, 183-223.

73. Li, L., Shin, O. H., Rhee, J. S., Arac, D., Rah, J. C., Rizo, J., Sudhof, T., and Rosenmund, C. (2006) *J Biol Chem* **281**, 15845-15852
74. Catz, S. D., Johnson, J. L., and Babior, B. M. (2002) *Proc Natl Acad Sci U S A* **99**, 11652-11657
75. Dunn, R., Klos, D. A., Adler, A. S., and Hicke, L. (2004) *J Cell Biol* **165**, 135-144
76. Domin, J., Gaidarov, I., Smith, M. E., Keen, J. H., and Waterfield, M. D. (2000) *J Biol Chem* **275**, 11943-11950
77. Yu, J. W., Mendrola, J. M., Audhya, A., Singh, S., Keleti, D., DeWald, D. B., Murray, D., Emr, S. D., and Lemmon, M. A. (2004) *Mol Cell* **13**, 677-688
78. Winters, M. J., Lamson, R. E., Nakanishi, H., Neiman, A. M., and Pryciak, P. M. (2005) *Mol Cell* **20**, 21-32
79. McLaughlin, S., Wang, J., Gambhir, A., and Murray, D. (2002) *Annu Rev Biophys Biomol Struct* **31**, 151-175
80. Beck, K. A., and Keen, J. H. (1991) *J Biol Chem* **266**, 4442-4447
81. Voglmaier, S. M., Keen, J. H., Murphy, J. E., Ferris, C. D., Prestwich, G. D., Snyder, S. H., and Theibert, A. B. (1992) *Biochem Biophys Res Commun* **187**, 158-163
82. Hao, W., Tan, Z., Prasad, K., Reddy, K. K., Chen, J., Prestwich, G. D., Falck, J. R., Shears, S. B., and Lafer, E. M. (1997) *J Biol Chem* **272**, 6393-6398
83. Wenk, M. R., and De Camilli, P. (2004) *Proc Natl Acad Sci U S A* **101**, 8262-8269
84. Medkova, M., and Cho, W. (1999) *J Biol Chem* **274**, 19852-19861.
85. Stahelin, R. V., Digman, M. A., Medkova, M., Ananthanarayanan, B., Rafter, J. D., Melowic, H. R., and Cho, W. (2004) *J Biol Chem* **279**, 29501-29512
86. Engh, R. A., and Huber, R. (1991) *Acta Crystallogr A* **47**, 392-400

FOOTNOTES

*This work was supported by National Institutes of Health grants GM68849 (W.C.) and by the Medical Research Council (R.L.W.)

[1]The abbreviations used are: CHAPS, (3-[3-cholamidopropyl) dimethylammonio]-1-propane-sulfonate; POPA, 1-palmitoyl-2-oleoyl-*sn*-glycero-3-phosphatidic acid; POPC, 1-palmitoyl-2-oleoyl-*sn*-glycero-3-phosphocholine; POPE, 1-palmitoyl-2-oleoyl-*sn*-glycero-3-phosphoethanolamine; POPS, 1-palmitoyl-2-oleoyl-*sn*-glycero-3-phosphoserine; PA, phosphatidic acid; PI, phosphoinositide; PS, phosphatidylserine; PtdIns3P, phosphatidylinositol-3-phosphate; PtdIns4P, phosphatidylinositol-4-phosphate; PtdIns5P phosphatidylinositol-5-phosphate; PtdIns(3,4)P_2, phosphatidylinositol-3,4-bisphosphate; PtdIns(3,5)P_2, phosphatidylinositol-3,5-bisphosphate; PtdIns(4,5)P_2, phosphatidylinositol-4,5-bisphosphate, PtdIns(3,4,5)P_3, phosphatidylinositol-3,4,5-trisphosphate; PLD1, phospholipase D1; PX, phox homology; PH, pleckstrin homology domain: PCR, polymerase chain reaction; RU, resonance unit; SPR, surface plasmon resonance.

FIGURE LEGENDS

Fig. 1. **PI3K-C2α PX domain overall structure.** *A*, A ribbon diagram of the overall fold of the PI3K-C2α PX domain colored from blue at the N-terminus to red at the C-terminus. *B,* Superposition of the Cα trace of the PI3K-C2α PX domain (red) on the p40^{phox} PX domain (green). The disordered PP_{II}/α2 loop in the PI3K-C2α PX domain is represented by the dashed line. Molecular illustrations were prepared using the program PyMOL (http://www.pymol.org).

Fig. 2. **Phosphoinositide binding pocket of PI3K-C2α.** *A,* A solid surface of the PI3K-C2α PX domain showing the lipid-binding pocket. The PtdIns3P from the p40^{phox} PX domain structure is superimposed on the surface. The presence of Thr^{1462} (magenta) and Asp^{1464} (red) in place of Arg^{58} and Arg^{60} from the p40^{phox} PX domain preclude binding of a phosphoinositide headgroup with a 3-phosphate. Arg^{1503} (blue) is in the vicinity of the 4- and 5-OH groups of the phosphoinositide and is the principal ligand of the sulfate bound in the PI3K-C2α PX domain lipid-binding pocket. *B,* An expanded view of the lipid-binding pocket with the p40^{phox} PX domain (green) superimposed on the Grd19 PX domain (salmon) and the PI3K-C2α PX domain (white). Despite the variation in conformation in the PP_{II}/α2 loop, the residue analogous to Lys^{92} of the p40^{phox} PX domain is the 1-phosphate ligand for both Grd19 and p40^{phox}. This suggests that the analogous residue in the PI3K-C2α PX domain, Arg^{1488}, may also be the 1-phosphate ligand. The polyproline loop (PP_{II}) of PI3K-C2α is highlighted as a yellow tube. The N- and C-terminal regions of the domains away from the PI-binding pocket have been removed for clarity. The dashed line joining the end of the PP_{II} to helix α2 emphasizes the disordered region of the PI3K-C2α PI-binding pocket.

Fig. 3. **Phosphoinositide specificity of the PI3K-C2α PX domain.** The PX domain (500 nM) was injected over a POPC/POPE/PI (78:20:2) surface to gauge affinity and specificity for different PIs, including PtdIns3P, PtdIns4P, PtdIns5P, PtdIns(3,4)P_2, PtdIns(3,5)P_2, PtdIns(4,5)P_2, and PtdIns(3,4,5)P_3. The SPR response curves for respective PI are shown after background correction for binding to the control surface coated with POPC/POPE (80:20). Binding to the control surface was minimal and little evidence of nonspecific binding was evident at 500 nM of protein.

Fig. 4. **Equilibrium SPR binding analysis of PI3K-C2α PX.** *A,* The PI3K-C2α PX domain was injected at 2 μl/min at varying concentrations (2, 5, 10, 20, and 60 nM from bottom to top) over the POPC/POPE/PtdIns(4,5)P_2 (78:20:2) surface and R_{eq} values were measured. *B,* A binding isotherm was generated from the R_{eq} (average of triplicate measurements) versus the concentration of the PI3K-C2α PX

domain plot. A solid line represents a theoretical curve constructed from R_{max} (= 170 ± 2) and K_d (= 25 ± 4 nM) values determined by nonlinear least-squares analysis of the isotherm using an equation: $R_{eq} = R_{max}/(1 + K_d/C)$. 10 mM HEPES buffer, pH 7.4, with 0.16 M KCl was used for all measurements.

Fig. 5. **Monolayer penetration analysis of PI3K-C2α PX domain.** *Δπ* was measured as a function of π_0 for wild type PI3K-C2α PX domain with POPC/POPE (80:20) (○), POPC/POPE/PtdIns(4,5)P_2 (78:20:2) (●), POPC/POPE/POPS (60:20:20) (□) and POPC/POPE/PtdIns(3,4)P_2 (78:20:2) (Δ), and POPC/POPE/PtdIns(3,4,5)P_3 (78:20:2) (■) monolayers. The subphase was 10 mM HEPES buffer, pH 7.4 containing 0.16 M KCl for all experiments. Each data represents average of duplicate measurements.

Fig. 6. **Monolayer penetration analysis of PI3K-C2α PX domain mutations.** *A, Δπ* was measured as a function of π_0 for POPC/POPE/PtdIns(4,5)P_2 (78:20:2) with wild type PI3K-C2α PX domain (○), K1440A (◆), R1488A (●), K1497A (▲), and R1503A (■). *B, Δπ* was measured as a function of π_0 for POPC/POPE/PtdIns(4,5)P_2 (78:20:2) with wild type PI3K-C2α PX domain (○), L1479A (□), V1490A (Δ), and L1491A. The subphase was 10 mM HEPES buffer, pH 7.4 containing 0.16 M KCl for all experiments. Each data represents average of duplicate measurements.

Fig. 7. **Phosphoinositide specificity of the PI3K-C2α C2 domain.** The C2 domain (500 nM) was injected over a POPC/POPE/PI (75:20:5) surface to estimate affinity and specificity for different PIs. The SPR response curves for respective PI are shown after background correction for binding to the control surface coated with POPC/POPE (80:20). Binding to the control surface was minimal at 500 nM of protein.

Fig. 8. **Membrane binding of the C2 and PX domains as a function of PtdIns(4,5)P_2 concentration.** Maximum binding response (R_{max}) of PX and C2 domains for the surface coated with POPC/POPE/PtdIns(4,5)P_2 (80-*x*:20:*x*) vesicles, where *x* is the concentration of PtdIns(4,5)P_2. Each data represents average of triplicate measurements.

Fig. 9. **Monolayer penetration analysis of PI3K-C2α and its isolated domains.** *A, Δπ* was measured as a function of π_0 for the PI3K-C2α C2 domain with POPC/POPE (80:20) (●), POPC/POPE/PtdIns(4,5)P_2 (78:20:2) (◆), and POPC/POPE/PtdIns(3,4)P_2 (78:20:2) (▲), and POPC/POPE/PtdIns(3,4,5)P_3 (78:20:2) (■) monolayers. PI3K-C2α PX domain (○) is also shown as a control. *B, Δπ* was measured as a function of π_0 using a POPC/POPE/PtdIns(4,5)P_2 (78:20:2) monolayer for the full-length PI3K-C2α●), R1503A (■), and PI3K-C2α PX domain (▲). The penetration of the full-length PI3K-C2α into a POPC/POPE (80:20) monolayer is also shown as a control (○). The subphase was 10 mM HEPES buffer, pH 7.4 containing 0.16 M KCl for all experiments. Each data represents average of duplicate measurements.

Table I.
Data collection, structure determination and refinement statistics

A. Data collection statistics

Crystal	Native(1)[a]	Native(2)[a]	EMTS derivative[a]
Resolution	2.9 Å	2.6 Å	2.6 Å
Completeness (last shell)	99.9 (100.0)	100.0 (100.0)	100.0 (100.0)
R_{merge}[b] (last shell)	0.060 (0.26)	0.094 (0.48)	0.10 (0.56)
Multiplicity (last shell)	40.4 (42.1)	41.0 (42.6)	7.1 (7.1)
$< I/\sigma >$ (last shell)	56.2 (12.8)	45.1 (6.5)	34.0 (2.9)
Unit Cell (Space group P423)	*a*=116.03	*a*=115.90	*a*=116.47

[a]Data sets were collected at ESRF beamline ID14-2 at λ=0.933 Å using a MAR CCD detector.
The single isomorphous replacement phasing and initial model building was carried out using native(1). Subsequently, a higher resolution native data set (2) was collected and used for refinement.

[b] $R_{merge} = \frac{\sum_{hkl}\sum_{i}\left|I_i(hkl) - \langle I(hkl)\rangle\right|}{\sum_{hkl}\sum_{i} I_i(hkl)}$

B. Phasing statistics

Phasing power (iso)[c]	1.8
Phasing power (anom)[c]	3.4
Hg sites found	3
FOM after SHARP	0.56
FOM after SOLOMON	0.82
FOM after DM	0.93

[c]The ratio of the heavy atom structure factor amplitudes to the the lack-of-closure error.

C. Refinement statistics

Resolution range	116 Å –2.6 Å
Number of reflections	7835
Cutoff (F/σ)	None
Completeness	99.97%
Protein atoms	2098
Number of TLS groups	5
Average total B factor after TLSANL (Wilson B factor)	59 Å^2 (67 Å^2)
Waters	9
R_{cryst}[d]	0.25
R_{free}[d] (% data used)	0.29 (10)
r.m.s.d. from ideality[e]	
bonds	0.016 Å
angles	1.7°
dihedrals	7.2°

[d] R_{cryst} and $R_{free} = \frac{\sum_{hkl}\left||F_{obs}| - |F_{calc}|\right|}{\sum_{hkl}|F_{obs}|}$; R_{free} calculated with the percentage of the data shown in parentheses.

[e]r.m.s. deviations for bond angles and lengths in regard to Engh and Huber parameters (86)

TABLE II

Binding parameters for PI3K-C2α PX domain and mutants determined from SPR analysis

Values represent the mean and standard deviation from three determinations. All measurements were performed in 10 mM HEPES, pH 7.4, containing 0.16 M KCl. Lipid vesicles were POPC/POPE/PtdIns(4,5)P_2 (75:20:2).

Protein	K_d (nM)	Fold increase in K_d [a]
PI3K-C2α PX domain	(2.5 ± 0.4) x 10^{-8}	1
K1440A	(2.9 ± 0.5) x 10^{-8}	1.2
L1479A	(3.0 ± 0.2) x 10^{-8}	1.2
R1488A	(1.8 ± 0.4) x 10^{-7}	7
V1490A	(1.7 ± 0.2) x 10^{-7}	7
L1491A	(1.3 ± 0.1) x 10^{-7}	5
R1493A	(5.7 ± 0.6) x 10^{-7}	23
K1497A	(3.4 ± 0.8) x 10^{-8}	1.4
R1503A	ND[b]	-

[a]Increase in K_d compared to K_d for wild type PX domain; [b]Not detectable.

TABLE III

Binding affinities of PI3K-C2α C2 and PX domains for different lipid vesicles.

Values represent the mean and standard deviation from three determinations. All measurements were performed in 10 mM HEPES, pH 7.4, containing 0.16 M KCl.

Protein	Lipid composition (78:20:2)	K_d (nM)	Fold increase in K_d[a]
PI3K-C2α PX domain	POPC/POPE/PtdIns(4,5)P_2	25 ± 4	1.0
Full-length PI3K-C2α	POPC/POPE/PtdIns(4,5)P_2	20 ± 3	0.8
R1503A PI3K-C2α	POPC/POPE/PtdIns(4,5)P_2	500 ± 33	20
PI3K-C2α C2 domain	POPC/POPE/PtdIns(4,5)P_2	490 ± 22	[b]20
PI3K-C2α C2 domain	POPC/POPE/PtdIns(3,4)P_2	510 ± 27	20
PI3K-C2α C2 domain	POPC/POPE/PtdIns(3,4,5)P_3	580 ± 39	23
PI3K-C2α C2 domain	POPC/POPE/PtdIns4P	950 ± 58	38

[a]Fold increase in K_d relative to the binding of the isolated PI3K-C2α PX domain.

[b]Notice that the C2 domain has 20-fold lower affinity than the PX domain under the same conditions.

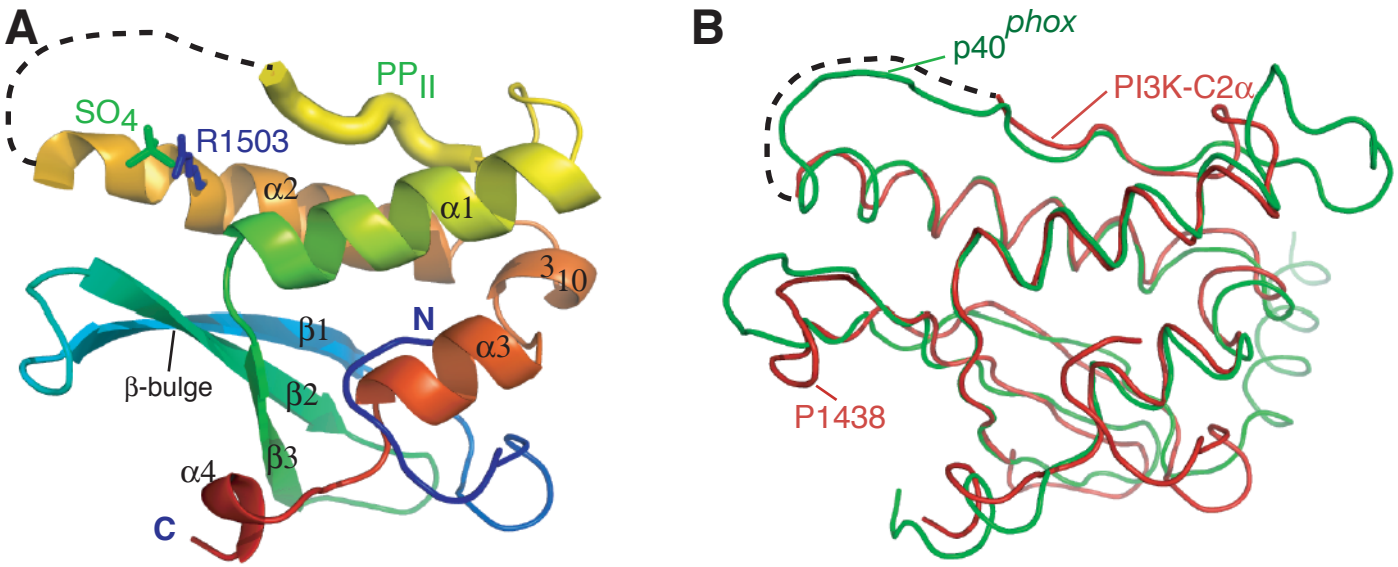

Fig. 1

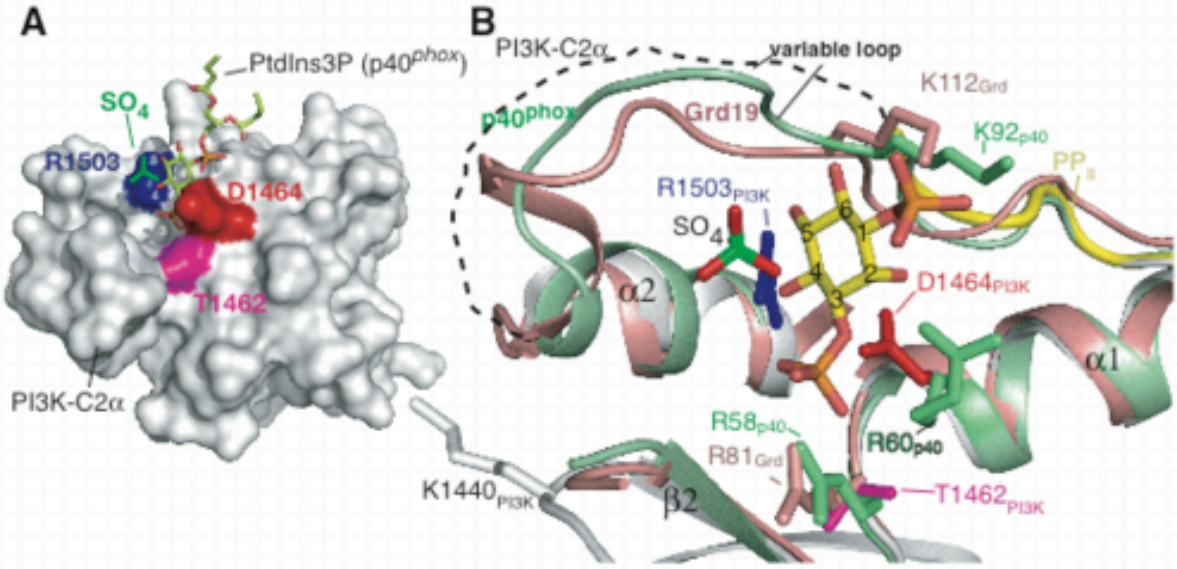

Fig. 2

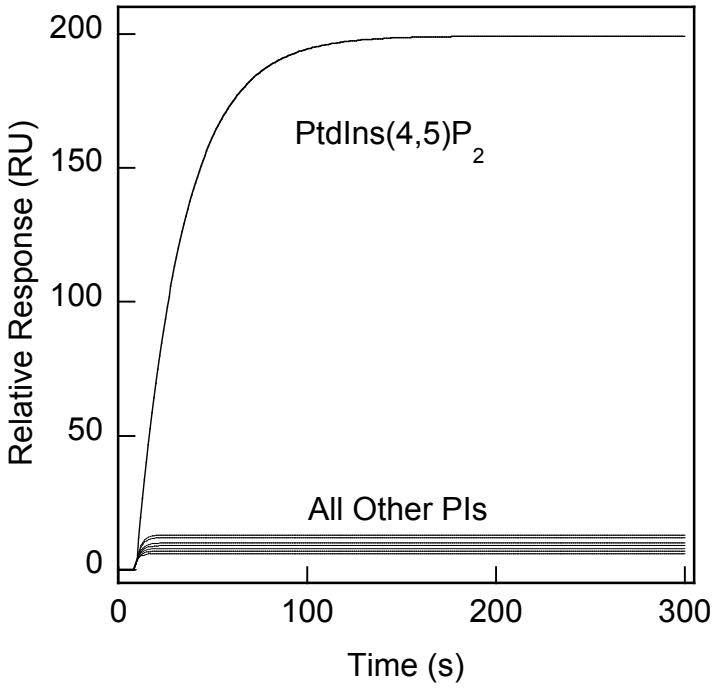

Fig 3

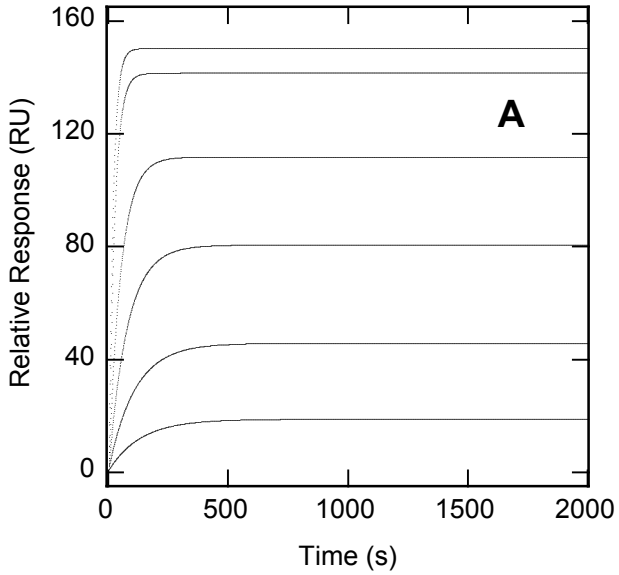

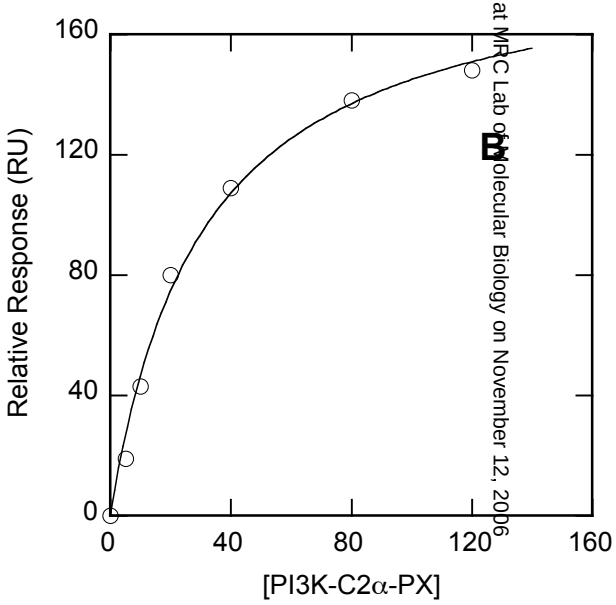

Fig 4

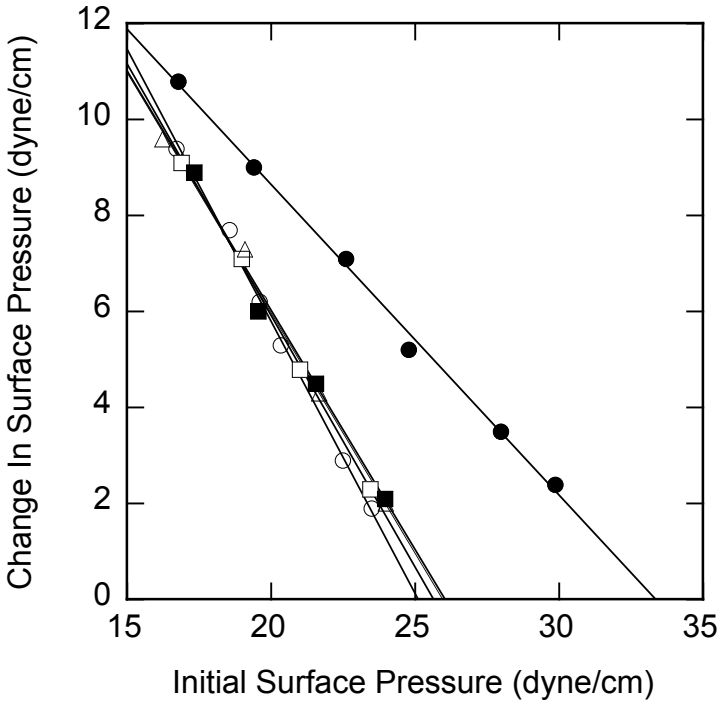

Fig 5

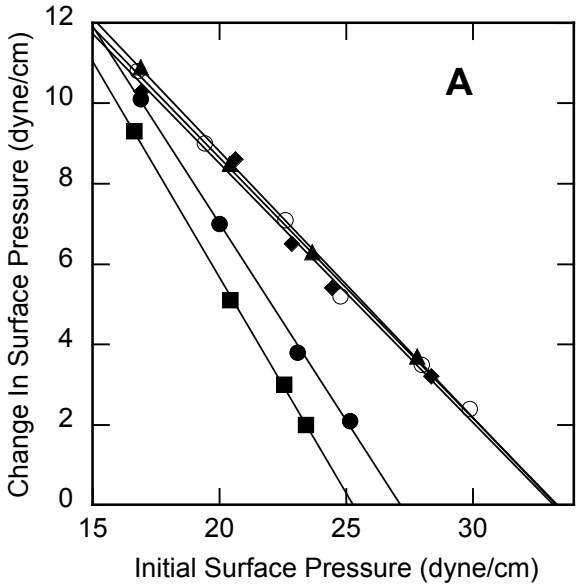

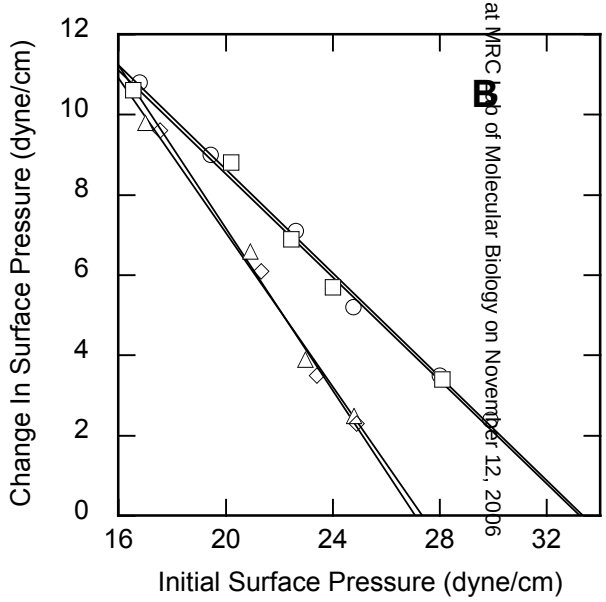

Fig 6

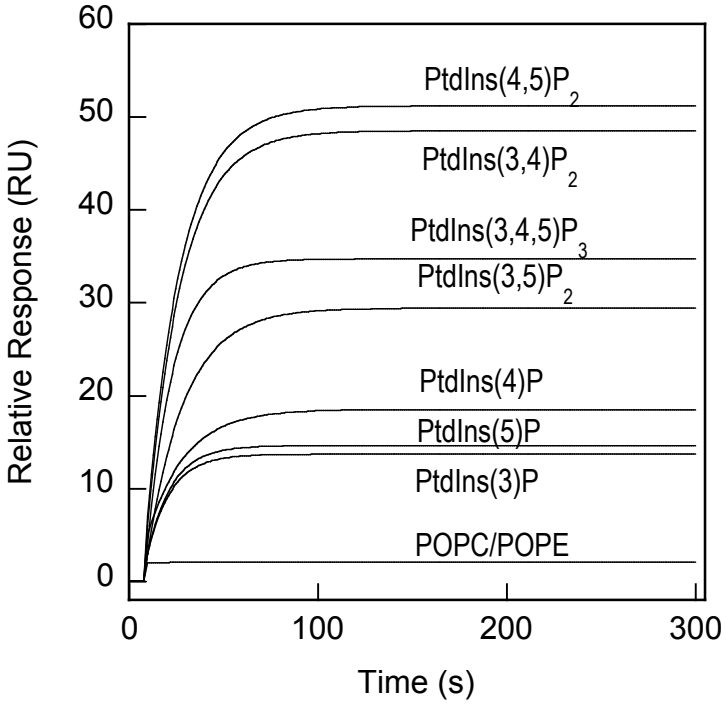

Fig 7

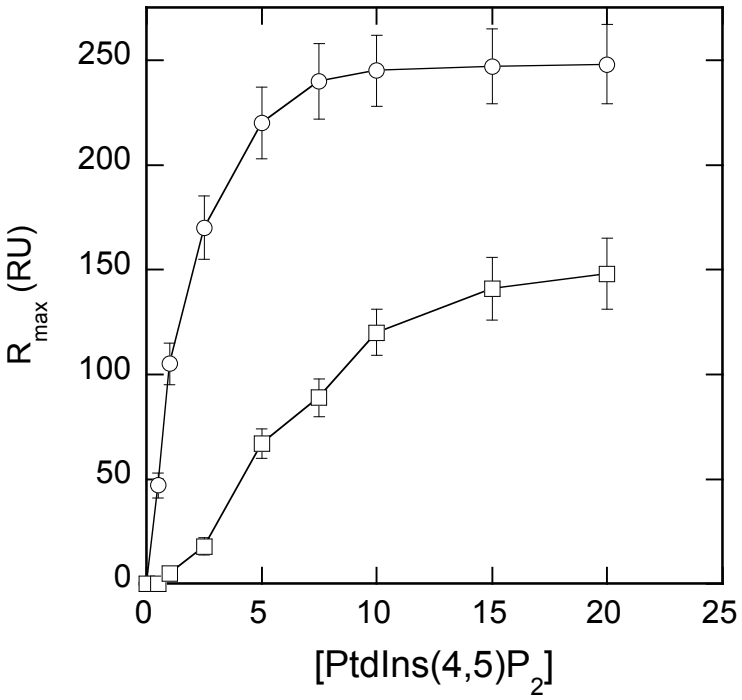

Fig 8

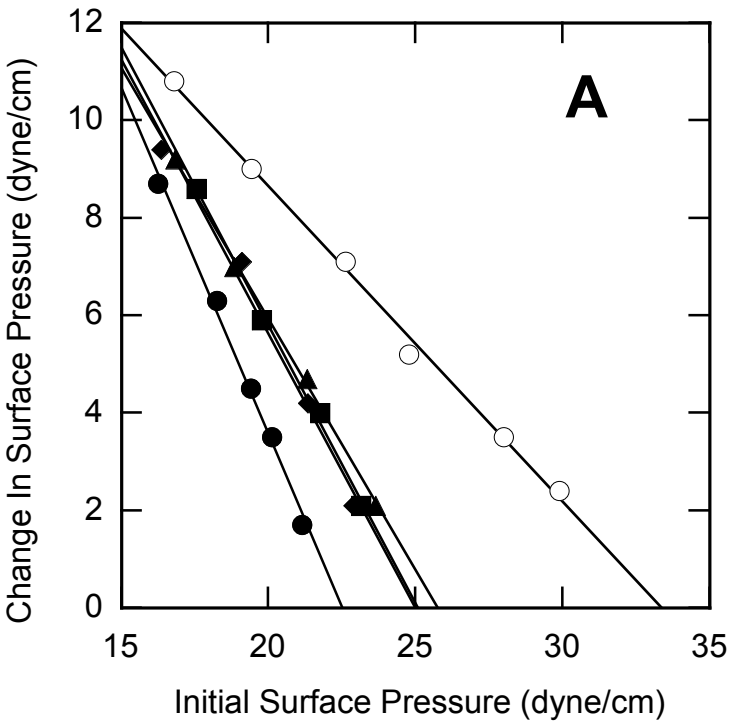

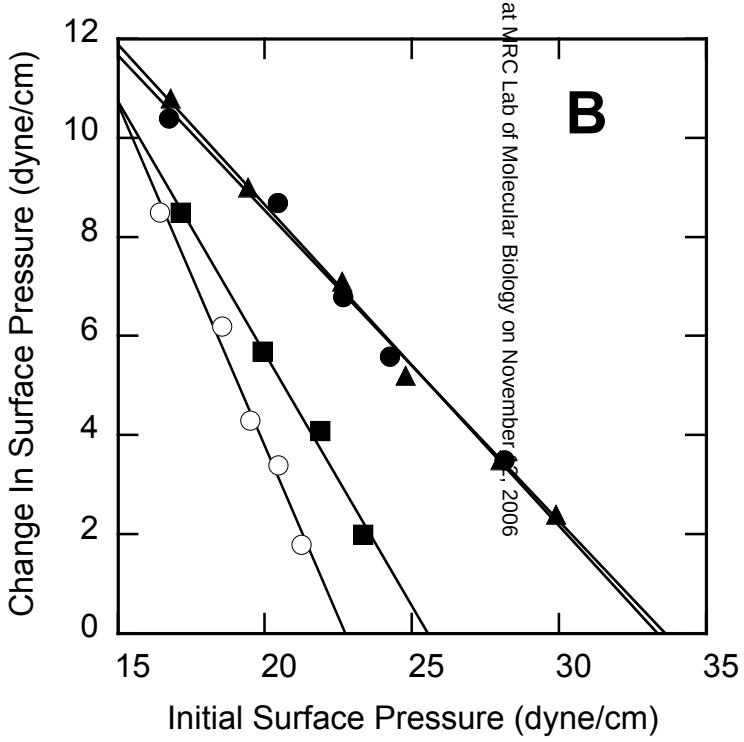

Fig 9